Seasonal dynamics of closed shallow lakes nutrient status controlled by lacustrine groundwater discharge

Xiaoliang Sun[1,2], Yao Du[1,2*], Hao Tian[1,2], Jiawen Xu[1,2], Huanhuan Shi[1,2], Yetong Liu[1,2], Yamin Deng[1,2], Yiqun Gan[1,2], Yanxin Wang[1,2]

[1]Key Laboratory of Groundwater Quality and Health (China University of Geosciences), Ministry of Education, Wuhan 430078, China.

[2]School of Environmental Studies & State Key Laboratory of Geomicrobiology and Environmental Changes, China University of Geosciences, Wuhan 430078, China.

Corresponding: Yao Du (yaodu@cug.edu.cn)

Abstract. Lacustrine groundwater discharge (LGD) and its associated nitrogen (N) and phosphorus (P) inputs are increasingly recognized as the critical drivers of lake eutrophication. However, the intermonthly variability in LGD and its influence on lake nutrient dynamics remain poorly understood. In this study, high-frequency monitoring and hydrochemical analyses were conducted over a full hydrological year to investigate LGD-related nutrient fluxes and their effects in a typical oxbow lake in the central Yangtze Basin. Water level data and ^{222}Rn tracing revealed a seasonal LGD pattern characterized by an increase from summer to winter, followed by a decline from winter to spring, with LGD rates ranging from 35.36 to 51.71 $mm \cdot d^{-1}$. This pattern was regulated by monthly net precipitation, which controlled the lake level fluctuations and LGD rates. The corresponding N and P loads varied synchronously with LGD and showed seasonal synchrony with lake N and P concentrations. Moreover, variations in the N/P ratio carried by LGD regulate the lake water N/P ratio, thereby influencing its relationship with the dynamic changes in chlorophyll-a. A large number of typical closed shallow lakes similar to the studied cases exist worldwide, and therefore, the regulatory role of LGD on lake nutrient status revealed in this study can be reasonably extended to other closed shallow lake systems. This study provides the first evidence that groundwater-driven nutrient loading influences lake nutrient status on an intermonthly scale, offering new insights and management strategies for eutrophication control in closed shallow lake systems worldwide.

1 Introduction

Lakes are vital terrestrial ecosystems with ecological, environmental, and societal importance (Zedler and Kercher, 2005). A number of studies have highlighted that lacustrine groundwater discharge (LGD) not only sustains the lake water balance but also serves as a key pathway for nitrogen (N) and phosphorus (P) inputs, significantly influencing biogeochemical cycling (Meinikmann et al., 2015; Rosenberry et al., 2015; Luo et al., 2018; Kazmierczak et al., 2020; Lewandowski et al., 2024). By altering nutrient concentrations, LGD can regulate lake trophic status and contribute to eutrophication (Shi et al., 2022; Zheng et al., 2024). Thus, understanding LGD's impact on lake water environments is critical for elucidating eutrophication mechanisms.

The LGD rate exhibits pronounced temporal variability over the hydrological year, primarily influenced by meteorological and hydrological factors (Burnett et al., 2017; Shi et al., 2022; Sun et al., 2024). In relatively closed lake systems (lacking perennial surface river inflows or where inflowing runoff has minimal impact on hydrodynamics, water balance, or residence time), meteorological factors are generally the dominant drivers of LGD. However, the magnitude and direction of these influences vary regionally. For instance, in Taihu Lake, LGD shows a positive correlation with evaporation (Shi et al., 2022), whereas in coal mining subsidence lakes, both precipitation and evaporation exhibit negative correlations with LGD (Jiang et al., 2024). In permafrost regions, LGD is largely restricted to the summer thaw period (Walvoord & Striegl, 2007; Olid et al., 2022). Although previous studies have made progress, understanding of LGD dynamics at the monthly scale remains limited due to insufficient observational frequency. Most existing studies focus on extreme hydrological periods (wet and dry seasons) or adopt seasonal observations, thus lacking monitoring at higher temporal resolution. However, the responses of lake and groundwater levels to precipitation and evaporation typically occur on monthly timescales, making it difficult for low-frequency or seasonal observations to adequately capture the processes by which water-level variations regulate LGD. In particular, the mechanistic linkages along the precipitation/evaporation → lake/groundwater level → LGD pathway require systematic investigation.

In existing studies, groundwater is regarded not only as an important source of lake water recharge, but also as a major contributor of nitrogen and phosphorus inputs to lakes. In some lakes, LGD contributes more than 50%, and in certain cases, over 90% of the total nitrogen (N) and phosphorus (P) inputs often exceed those from surface inflows (Stets et al., 2010; Meinikmann et al., 2015; Shi et al., 2022). Once discharged, groundwater-derived nutrients undergo biogeochemical transformations or are

assimilated by aquatic organisms, thereby affecting the primary productivity and eutrophication (Zheng et al., 2025). For instance, LGD-driven nutrient inputs have been shown to stimulate chlorophyll a (Chl *a*) production in closed lakes and alter nutrient limitation patterns via shifts in N/P ratios (Xu et al., 2025). In Taihu Lake, LGD-derived N inputs were found to alleviate N limitation (Zheng et al., 2025). However, most studies have focused on nutrient flux quantification over discrete periods, with limited insight into the temporal variability and trophic responses of lakes. Understanding the monthly-scale variations and their controlling mechanisms is essential not only for predicting responses to extreme hydrological events but also for identifying critical periods of nutrient input that drive eutrophication.

Environmental tracers are increasingly applied in studies of LGD. An ideal tracer typically exhibits significant concentration differences between lake water and groundwater (often spanning orders of magnitude) and stable chemical properties (Arnoux et al., 2017; Petermann et al., 2018). Commonly used tracers include ^{222}Rn, ^{226}Ra, stable hydrogen and oxygen isotopes ($\delta^{2}H$, $\delta^{18}O$), Cl^-, and electrical conductivity (Sun et al., 2021). Among these, ^{222}Rn and ^{226}Ra often show concentration differences of up to two-three orders of magnitude between the two water types, whereas differences in Cl^- and electrical conductivity are generally smaller (sometimes only several times). Therefore, ^{222}Rn and ^{226}Ra are frequently the preferred tracers in LGD studies, with other indicators used as auxiliaries when conditions permit (Dimova & Burnett., 2011). The applicability of stable hydrogen and oxygen isotopes is strongly influenced by hydrological stability; in lakes with pronounced seasonal hydrological fluctuations, their quantitative accuracy may be significantly reduced (Sun et al., 2025a). Regarding radioactive tracers, ^{226}Ra primarily desorbs from particles into the water phase in brackish or saline environments (Webster et al., 1995; Gonneea et al., 2008), and its concentration is typically low in freshwater lakes. Consequently, in freshwater lake LGD studies, ^{222}Rn is more commonly used and effective due to its high solubility, large concentration gradient, and ease of detection.

The middle Yangtze River plain is characterized by a high density of lakes, and previous studies have shown that lakes of different types commonly exhibit groundwater discharge of varying intensities, along with associated nitrogen and phosphorus input fluxes (Jiang et al., 2022; Hu et al., 2023; Gan et al., 2023). However, its specific role in nutrient loading and eutrophication remains poorly understood. Heiwawu Oxbow Lake (HW lake), situated along a former Yangtze River channel, provides a valuable setting to examine the temporal dynamics of LGD due to its seasonal hydrological connectivity. Typically isolated from the Yangtze by November, HW lake experienced an earlier

disconnection in August 2022 due to extreme drought (Sun et al., 2024). During this period, the lake's water and nutrient balance depended almost entirely on precipitation and groundwater, offering an ideal natural experiment to investigate LGD-driven nutrient loading and eutrophication over a complete hydrological year.

In this study, we quantified LGD and its associated nitrogen and phosphorus fluxes by conducting bi-monthly, high-frequency monitoring of groundwater and lake water levels, and by applying a ^{222}Rn mass balance model to a typical closed lake in the middle reaches of the Yangtze River. Furthermore, we examined the influence of meteorological factors on LGD and the dynamic effects of LGD-driven nutrient inputs on lake trophic status. The results elucidate the role of precipitation and evaporation in regulating the seasonal dynamics of LGD and highlight the critical influence of LGD on the nutrient regime of closed lakes. These findings provide a valuable scientific basis for improving water quality management and mitigating eutrophication in closed-lake systems worldwide.

2 Materials and Methods

2.1 Study area

HW lake is situated in the southern Jianghan Plain on the northern bank of the middle reaches of the Yangtze River, between 29° 45' 10.98'' – 29° 48' 52.10'' N and 112° 41' 35.90'' – 112° 46' 32.16'' E (Figure 1a and b). The region has a subtropical monsoon climate, with an annual mean temperature of 15–17°C, average annual precipitation of approximately 1400 mm, and average annual evaporation of approximately 1100 mm. HW lake was formed in 1967 following the artificial cutoff of a meander of the Yangtze River, with a downstream channel providing hydrological connectivity between the lake and the river. During the wet season, elevated Yangtze River water levels induce the inflow into HW lake, whereas in the dry season, declining Yangtze River levels result in backflow from the lake into the river, ultimately leading to complete disconnection. In a typical hydrological year, HW lake experiences substantial water level fluctuations between the wet and dry seasons, with a magnitude of up to 8 m.

The aquifer interacting with the oxbow lake comprises two distinct layers (Figure 1c). The upper layer with 5–15 m thickness consists of low-permeability clay and silty clay with a hydraulic conductivity of approximately 1 $m \cdot d^{-1}$. In contrast, the lower layer is a confined aquifer 50–80 m thick, composed mainly of fine to coarse sand, and exhibits a higher hydraulic conductivity of approximately 5–15 $m \cdot d^{-1}$. Owing to its greater permeability, the lower aquifer functions as the primary groundwater

source directly connected to the lake. Previous studies have confirmed substantial LGD in HW lake, predominantly occurring as springs (Figure 1 d1–d6) and seepage flows (Sun et al., 2025b). The area surrounding HW lake is characterized by flat terrain with a slope of less than 0.1‰, and the dominant land use types include forest and farmland. This indicates that, except for runoff through artificial channels, surface runoff generated by other precipitation is almost negligible, and the water level gradient, rather than the terrain slope, becomes the key factor controlling groundwater-lake water exchange.

In 2022, a severe drought event in Yangtze River caused the water level of HW lake to decline in parallel with that of the Yangtze River, ultimately leading to complete disconnection from the river. Consequently, the lake entered the dry season approximately two months earlier than that in a typical hydrological year. During the groundwater discharge period, the water level of HW lake was minimally affected by hydrological fluctuations in the Yangtze River and was instead primarily controlled by meteorological factors such as precipitation and evaporation.

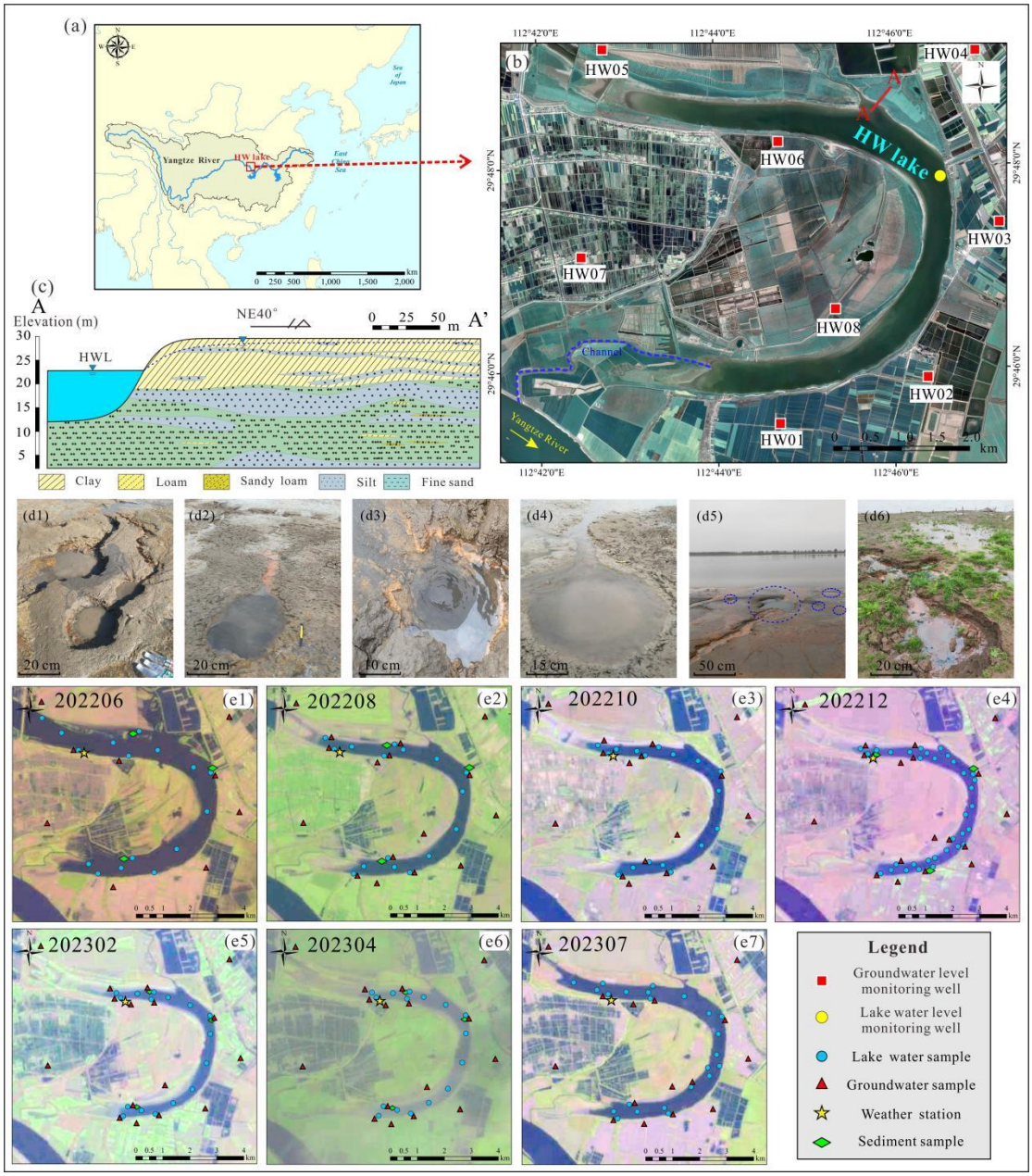

Figure 1. Overview of the study area. (a) Geographical location of the HW lake (study area marked by a red box, from Esri). (b) satellite image of HW lake (from Google Maps). (c) Hydrogeological cross-section along profile A–A' (profile location indicated by line A–A' in b). The cross-section shows only the upper part of the confined aquifer that interacts with the lake, and does not display the full thickness of the aquifer. (d1–d6) Zones of concentrated LGD phenomena in HW lake, primarily manifested as spring outlets. (e1–e7) Spatial distribution of field sampling sites collected between June and July 2022 (from Landsat 8). The numbers in the figure indicate the sampling periods. For example, 202208 represents August 2022. In June 2022 and July 2023, HW lake was connected to the Yangtze River through a channel, receiving inflow from the river, which led to higher water levels and an expanded inundated area. In the other months, HW lake was isolated from the Yangtze River, representing the period when LGD occurred.

2.2 Field work and laboratory analysis

Systematic field sampling was conducted from June 2022 to July 2023, with a sampling frequency

of once every two months. Except for the July 2023 sampling conducted in early July, all other campaigns were performed at the end of the even-numbered months. Except for the campaigns in June 2022, December 2022, and July 2023, all sessions followed a standardized protocol involving the collection of 16 lake water samples, 8 well water samples, and 8 pore water samples. A total of 241 samples were collected (Table 1, Figure 1 e1–e7), comprising 135 lake water samples, 56 well water samples, and 50 pore water samples. In addition to sample collection, each campaign included simultaneous measurements of environmental parameters, such as groundwater level, lake water level, lake depth, and wind speed. Due to seasonal fluctuations in lake water levels, the shoreline position shifted over time, resulting in slight spatial variations in the lakeshore sampling points across campaigns. The wind speed was continuously recorded at 15-min intervals using a weather station installed on the lakeshore, while the precipitation and evaporation data were sourced from the ECMWF reanalysis datasets.

Table 1. Number of samples per sampling campaign.

Time	Number of lake water samples	Number of well water samples	Number of pore water samples	Total
June 23–29, 2022	16	8	2	26
August 26–30, 2022	16	8	8	32
October 26–31, 2022	16	8	8	32
December 17–30, 2022	35	8	10	53
February 20–25, 2023	16	8	8	32
April 23–27, 2023	16	8	8	32
July 6–14, 2023	20	8	6	34
Total	135	56	50	241

Samples from the lake center were collected by boat at fixed preselected locations. Surface water was sampled approximately 0.5 m below the surface using a specialized surface water sampler. The groundwater samples were categorized into two types: (1) well water collected from monitoring wells located 0.5 to 2.5 km from the lakeshore, with the depths between 15 and 30 m, and (2) spring water collected from natural springs situated within 15 m of the shoreline and in shallow lake zones, serving as the representative lakeshore pore water. In addition, three nearshore lakebed sediment samples were collected for incubation experiments to determine the ^{222}Rn concentrations. The wind speed was continuously recorded at 15-min intervals using a weather station installed on the lakeshore, while the precipitation and evaporation data were sourced from the ECMWF reanalysis datasets.

For ^{222}Rn analysis, the water samples were collected in 250 mL or 2.5 L glass bottles using an overflow method to eliminate residual air. ^{222}Rn concentrations were quantified using a RAD7 system

(Durridge Company, Inc.) equipped with RAD7-H_2O and RAD7 Big Bottle accessories. To reduce the measurement uncertainty in lake water samples, the counting time was extended to 60 min per sample. All ^{222}Rn analyses were completed within 24 h of sampling, using the RAD7 aqueous system.

$$A_0 = A \times e^{\lambda t} \quad (1)$$

where A_0 represents the ^{222}Rn concentration ($Bq \cdot m^{-3}$) at the sampling time; A represents the ^{222}Rn concentration ($Bq \cdot m^{-3}$) at the measurement time; λ represents the decay coefficient of ^{222}Rn, 0.181 d^{-1}; and t represents the time interval (d) between sampling and measurement. The uncertainty in ^{222}Rn testing for lake water was approximately 35%, and the uncertainty in ^{222}Rn testing for groundwater is approximately 25%.

The samples for total nitrogen (TN) and total phosphorus (TP) analysis were field-filtered using a 0.45 μm membrane filter and then stored in 30 mL polyethylene bottles and 20 mL brown screw-cap glass bottles, respectively. The TP samples were acidified with concentrated HNO_3 to a pH below 2, sealed, and subsequently analyzed using an inductively coupled plasma optical emission spectrometer (ICP-OES, iCAP 6000 series, Thermo Fisher Scientific, USA) at the School of Environmental Studies, China University of Geosciences (Wuhan), with a detection limit of 0.001 $mg \cdot L^{-1}$. TN samples were analyzed using a total organic carbon/nitrogen analyzer at the Wuhan Botanical Garden, Chinese Academy of Sciences, with a detection limit of 0.01 $mg \cdot L^{-1}$. Chl *a* concentrations were determined immediately after sampling using an AquaFluor fluorometer, with a detection limit of 0.5 $\mu g \cdot L^{-1}$. Water quality parameters, including pH, temperature, DO, ORP, and EC, were measured in situ using a HACH-HQ40D multi-parameter probe.

2.3. ^{222}Rn mass balance model

In recent years, ^{222}Rn has been widely used in studies of LGD. Derived from its parent isotope ^{226}Ra, ^{222}Rn has a half-life of 3.82 d. By treating lake water as a closed system, a mass balance model was developed based on both the sources and sinks of ^{222}Rn. The ^{222}Rn flux from the groundwater discharge was inferred as an unknown term. The ^{222}Rn mass balance model is expressed as follows, and a conceptual diagram of its budget terms is shown in Figure S1:

$$\frac{\partial I^{222}Rn}{\partial t} = F_g + F_d + I^{226}Ra \times \lambda^{226}\mathrm{Ra} - F_a - I^{222}Rn \times \lambda^{222}Rn \quad (2)$$

where F_g, F_d, and F_a are the ^{222}Rn fluxes ($Bq \cdot m^{-2} \cdot d^{-1}$) of groundwater discharge, sediment diffusion, and atmospheric escape, respectively; $I^{226}Ra$ and $I^{222}Rn$ are the pools of ^{226}Ra and ^{222}Rn in the lake water ($Bq \cdot m^{-2}$), which are equal to the concentrations of ^{226}Ra and ^{222}Rn multiplied by the water depth; and the decay coefficients of ^{222}Rn ($\lambda^{222}Rn$) and ^{226}Ra ($\lambda^{226}Ra$) were 0.181 d^{-1} and 1.31 × 10^{-11} d^{-1}, respectively. The measurement times before and after sampling were the first day and the last day of the sampling period, respectively. Since there is almost no difference in the lake water level and ^{222}Rn concentration at the same location before and after sampling, the change in the ^{222}Rn in lake water on the left side of the equation can be approximated as 0 (Kluge et al., 2007).

The ^{222}Rn flux diffused from the sediment to the lake is one source of the ^{222}Rn mass balance model, and it is calculated by the following formula:

$$F_d = \sqrt{\left(\lambda^{222}Rn \times nD_m\right)}\left(C_p - C_w\right) \tag{3}$$

where C_p ($Bq \cdot m^{-3}$) and C_w ($Bq \cdot m^{-3}$) are ^{222}Rn concentrations of pore water in sediments and overlying lake water, respectively; D_m ($cm^2 \cdot s^{-1}$) is the ^{222}Rn molecular diffusion coefficient in wet bulk sediment; n is the porosity of the sediment.

To determine the ^{222}Rn concentrations in sediment pore water, a sediment equilibrium incubation experiment was carried out following the procedure proposed by Corbett et al. (1998). The D_m is expressed as:

$$-\log D_m = \left(\frac{980}{T_w + 273}\right) + 1.59 \tag{4}$$

where T_w is water temperature (°C). An equilibrium incubation experiment with lakebed sediments was carried out to obtain the ^{222}Rn concentration in sediment pore water (Corbett et al., 1998).

The atmospheric loss of ^{222}Rn is estimated based on the following empirical equation, which is related to temperature and wind speed (MacIntyre et al., 1995):

$$F_a = K\left(C_w - \alpha C_a\right) \tag{5}$$

where K values are in cm h^{-1} but have been scaled to $m \cdot d^{-1}$ for input into Eq. (5); C_w is the concentration of lake water ^{222}Rn ($Bq \cdot m^{-3}$); C_a is the concentration of ^{222}Rn in the air ($Bq \cdot m^{-3}$); α is the gas distribution coefficient (dimensionless) and is a temperature dependent function; ^{222}Rn from the decay of dissolved ^{226}Ra can be generally omitted for ^{222}Rn mass balance model.

The LGD rate can be obtained by dividing the ^{222}Rn flux from groundwater discharge by the ^{222}Rn

concentration of surrounding groundwater. The formula is as follows (Luo et al., 2018; Wang et al., 2019):

$$V = \frac{F_g}{C_g} \times 1000 \quad (6)$$

where V is the average LGD rate ($mm \cdot d^{-1}$); Fg is the ^{222}Rn flux of groundwater discharge ($Bq \cdot m^{-2} \cdot d^{-1}$) ; Cg is the ^{222}Rn concentrations in groundwater end member ($Bq \cdot m^{-3}$). A more detailed description can be found in Section 1 of the SI.

3 Results and Discussion

3.1 Seasonal variations in LGD rates

3.1.1 Identification of seasonal variations in LGD

1. Lake water and groundwater level

The fluctuations in lake water levels and groundwater levels reflect a pronounced interaction between groundwater and the lake. During the field monitoring period, both exhibited significant changes in water level.

From June 2022 to July 2023, the lake water level fluctuated significantly between 22.30 and 32.90 m, with a peak in late June 2022 and a low in late February 2023, demonstrating a variation of 10.6 m (Figure 2a). Initially, the HW lake's high water level was sustained by its connection to the Yangtze River, which was at a high level in June 2022. However, a severe drought from August to September 2022 caused a rapid decline in the Yangtze River level, resulting in a corresponding decrease in the HW lake level. From late October 2022 to early May 2023, as the Yangtze River fell below 26.5 m, HW lake became hydrologically isolated, with no surface water inflow or outflow. The rate of water level decline slowed from October 2022 to February 2023 and began to rise in March 2023 because of increased precipitation. In May 2023, when the Yangtze River exceeded 26.5 m again, the HW lake level rose sharply due to the inflow.

The groundwater levels from the eight surrounding wells exhibited similar fluctuations, ranging from 26.6 to 30.9 m (Figure 2a). From June 2022 to April 2023, groundwater levels consistently declined, with a slight increase observed from April to July 2023. Generally, the groundwater level trends mirrored those of the lake, except for the period from February to April 2023, when the groundwater levels decreased while the lake levels increased. The difference between the average groundwater and lake levels ranged from -1.98 to 4.45 m, affecting the LGD rates over time. In June

2022, all eight wells had groundwater levels lower than those of the lake, indicating complete lake recharge. By July 2023, four wells presented lower groundwater levels, whereas four exhibited higher levels, suggesting simultaneous recharge and discharge. From August 2022 to April 2023, groundwater consistently discharged into the lake, with the largest groundwater-lake level difference occurring in December 2022, indicating the highest LGD rate during that period (Figure 2b).

2. Lake water and groundwater ^{222}Rn concentration

As a limited tracer for LGD, the concentration of ^{222}Rn can indicate changes in LGD. During the field monitoring period, both lake water and groundwater concentrations underwent some variations, with differing magnitudes.

The fluctuation in the lake water ^{222}Rn concentration from June 2022 to July 2023 (Figure 2c) exhibited an initial increase followed by a decrease. The lowest concentration occurred in June 2022, whereas the highest was recorded in December 2022, with values of 87.50 and 231.61 $Bq \cdot m^{-3}$, respectively. Similarly, groundwater also demonstrated a trend of initial decrease followed by an increase (Figure 2d), with the highest values in June 2022 and the lowest values in April 2023, at 5863.45 and 2558.30 $Bq \cdot m^{-3}$ respectively.

During the period of groundwater discharge to the lake, when groundwater levels were consistently above lake levels (August 2022 to April 2023), the lake water ^{222}Rn concentration ranged from 106.83 to 231.61 $Bq \cdot m^{-3}$. While, the groundwater ^{222}Rn concentration ranged from 2558.30 to 3910.40 $Bq \cdot m^{-3}$. Based on the coefficient of variation (CV, used to measure the relative dispersion of data, defined as the ratio of the standard deviation to the arithmetic mean), the ^{222}Rn concentration in groundwater ($CV \approx 17.60\%$) is more stable than that in lake water ($CV \approx 26.62\%$), indicating a relatively consistent ^{222}Rn endmember value for groundwater. Because groundwater was the primary source of ^{222}Rn in the lake, variations in lake water ^{222}Rn concentrations reflected changes in the LGD rate. As shown in Figure 2e, the ratio of lake water to groundwater ^{222}Rn concentration initially increased and then decreased with a peak in December 2022, which suggested that the LGD rate was the highest during that period. This pattern is consistent with the relationship between groundwater and lake water levels.

Notably, as shown in Figure. 2a and c, during the two periods when the groundwater level was lower than the lake water level (June 2022 and July 2023), lake-water ^{222}Rn concentrations were 87.50

and 95.59 Bq m^{-3}, respectively, which are lower than those in the other periods, indicating that groundwater discharge was generally limited. Nevertheless, measurable ^{222}Rn was still detected in the lake water, suggesting additional inputs from other water sources. Concurrently, ^{222}Rn concentrations in the Yangtze River were 90.50 and 50.47 Bq m^{-3}, respectively. In June 2022, the lake-water ^{222}Rn concentration was very similar to that of the Yangtze River, indicating that the lake was mainly controlled by Yangtze River inputs during this period. In contrast, in July 2023 the lake-water ^{222}Rn concentration was slightly higher than that of the Yangtze River; together with the observation that groundwater levels in some monitoring wells were still slightly higher than the lake level, this suggests the presence of weak, localized groundwater discharge during this period. In addition, intense summer precipitation led to increased catchment runoff into the lake, which generally exhibited high ^{222}Rn concentrations, primarily derived from ^{222}Rn released through interactions between rainfall and surface soils rather than from aquifer groundwater. Overall, the higher lake-water ^{222}Rn concentration in July 2023 compared with June 2022 reflects the combined effects of Yangtze River input, localized weak groundwater discharge, and precipitation-driven runoff.

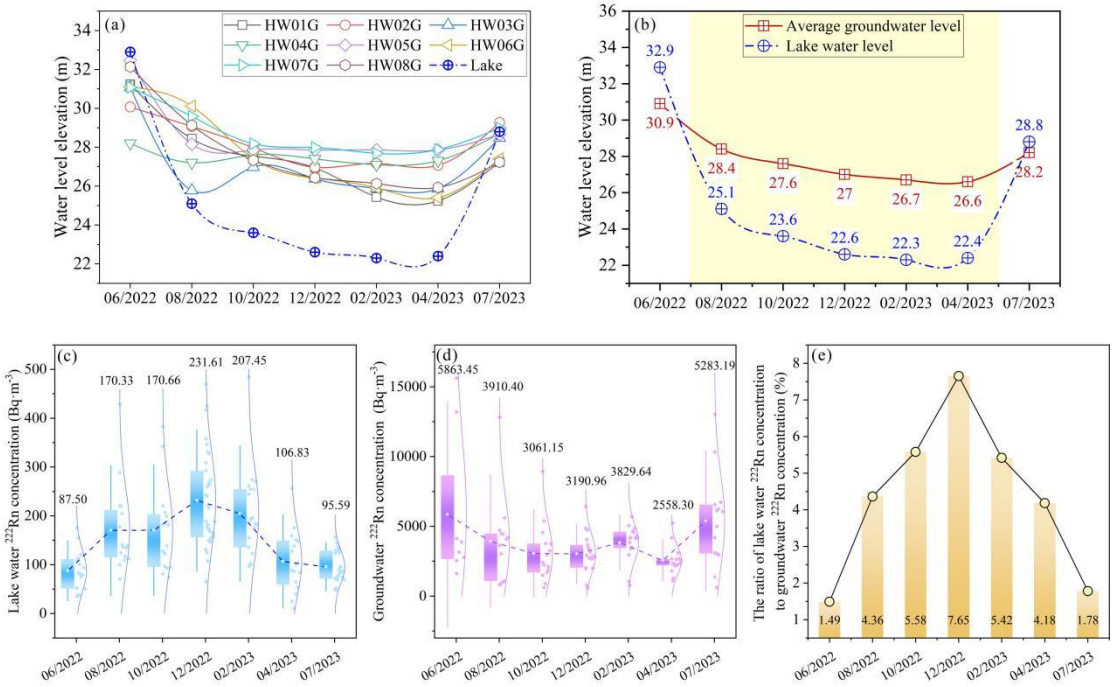

Figure 2. (a) Variations in lake water level and groundwater levels across all groundwater monitoring points. (b) Variations in lake water levels compared with the average groundwater level, the yellow area indicates the period of LGD. (c) Variations in the lake water concentrations of ^{222}Rn. (d) Variations in the groundwater concentrations of ^{222}Rn. In (c) and (d), the top and bottom of each box represent the 75th and 25th percentiles of the data, respectively; the ends of the whiskers indicate the maximum and minimum values within 1.5 times the interquartile range; the small white square inside the box denotes the mean; the side curves illustrate the data's dispersion and distribution pattern; the dark blue dashed line connects the mean values across different periods. (e) Variations in the ratio of ^{222}Rn concentrations in lake water to groundwater.

3.1.2 Quantification of LGD rates for each period

Based on the lake level and groundwater monitoring data, the period from late August 2022 to late April 2023 was characterized by consistently higher groundwater levels than the lake stage, during which the lake was hydrologically isolated from external surface water inputs. This interval was conservatively defined as the active phase of LGD (Figure 2b). Using the ^{222}Rn mass balance model, LGD rates were computed for each period of groundwater discharge during groundwater excretion.

Table 2 summarizes the detailed parameters and results for the source and sink terms across each sampling period. A comparison of the ^{222}Rn fluxes associated with the source and sink terms in the ^{222}Rn mass balance model for each period is shown in Figure S2. In terms of source, the groundwater-derived ^{222}Rn input flux ranged from 90.48 ± 36.32 to 165.02 ± 63.09 $Bq \cdot m^{-2} \cdot d^{-1}$, while the diffusive flux of ^{222}Rn from sediment pore water varied between 18.82 ± 2.88 and 21.51 ± 3.29 $Bq \cdot m^{-2} \cdot d^{-1}$. In terms of sink, the radioactive decay flux of ^{222}Rn in lake water ranged from 73.47 ± 26.74 to 163.49 ± 59.51 $Bq \cdot m^{-2} \cdot d^{-1}$, and atmospheric evasion accounted for a flux of 20.34 ± 6.46 to 38.51 ± 12.87 $Bq \cdot m^{-2} \cdot d^{-1}$.

The LGD rates for each period were calculated by dividing the flux of ^{222}Rn input from LGD by the corresponding groundwater ^{222}Rn concentration (Figure 3a). From August 2022 to April 2023, the LGD rates ranged from 35.36 ± 16.39 to 51.71 ± 23.23 $mm \cdot d^{-1}$, with the maximum value being 1.46 times the minimum value. Notably, an increasing trend in groundwater excretion rates was observed from August 2022 to December 2022, which was followed by a decreasing trend from December 2022 to April 2023. The highest rate of groundwater excretion occurred in December 2022, whereas the lowest LGD rate was recorded in April 2023.

Table 2. The calculation parameters and results of the ^{222}Rn mass balance model for each period.

	08/2022	10/2022	12/2022	02/2023	04/2023
Lake water ^{222}Rn concentration ($Bq \cdot m^{-3}$)	170.33 ± 88.71	170.66 ± 89.10	231.61± 96.53	207.45±98.16	106.83±63.85
Air ^{222}Rn concentration ($Bq \cdot m^{-3}$)	16.20	16.20	16.20	16.20	16.20
Wind speed above 2 m lake surface ($m \cdot s^{-1}$)	1.48±0.82	1.37±0.83	1.08±1.11	1.65±1.44	2.05±1.57
K ($m \cdot d^{-1}$)	0.30±0.02	0.17±0.01	0.08±0.01	0.16±0.01	0.34±0.01
Sc	554.34	937.71	1572.2	1492.73	871.45
Lake water temperature (℃)	29.19	18.43	8.86	9.78	19.89
Lake water depth (m)	4.9	4.2	3.9	3.8	3.8
Groundwater ^{222}Rnconcentration ($Bq \cdot m^{-3}$)	3910.40 ± 3511.38	3061.15± 2099.00	3028.17± 1412.72	3829.64± 1316.67	2588.30± 998.11
The ^{222}Rn flux of atmospheric escape	49.80±18.20	30.96±10.27	20.34±6.46	37.12±11.56	38.51±12.87

($Bq \cdot m^{-2} \cdot d^{-1}$)					
The ^{222}Rn flux of pore in sediment diffusion ($Bq \cdot m^{-2} \cdot d^{-1}$)	24.70±3.78	21.10 ± 3.23	18.82±2.88	18.74±2.87	21.51±3.29
The ^{222}Rn flux of decay ($Bq \cdot m^{-2} \cdot d^{-1}$)	151.07± 54.99	129.74±47.22	163.49±59.51	142.68±51.93	73.47±26.74
The ^{222}Rn flux of groundwater discharge ($Bq \cdot m^{-2} \cdot d^{-1}$)	176.16± 58.05	139.59±48.44	165.02± 63.09	161.06±60.63	90.48±36.32
LGDrate ($mm \cdot d^{-1}$)	45.05± 18.39	45.60± 34.20	51.71±23.23	42.06±18.60	35.36±16.39

335

336 **3.2 Climatic controls on seasonal variations in LGD rates**

337 **3.2.1 Relationship between precipitation and evaporation and LGD rates**

338 To obtain a higher temporal resolution within the hydrological year, fitting equations were
339 established to simulate the monthly LGD rates during groundwater discharge periods. The quadratic
340 equation representing LGD rates based on the ^{222}Rn mass balance model and time was $Y = -0.54X^2 +$
341 $6.42X + 29.82$, $R^2 = 0.83$, $P < 0.05$ (where X represents the time and Y represents the LGD rate)
342 (Figure 3a). Due to the small sample size, the robustness of the model's fit may be limited. Nonetheless,
343 under the field observed conditions, the monthly fluctuations of lake and groundwater levels were
344 relatively small and exhibited regular patterns, so the actual monthly variation of LGD showed a
345 predictable "increase followed by decrease" pattern. Therefore, the predictions of this model are
346 considered reliable. Using this equation, the LGD rates were estimated for the period from August 2022
347 to May 2023. Although the water level at the Jianli station of the Yangtze River exceeded 26.5 m in
348 May 2023 for just 10 d, the inflow from the Yangtze River to the HW lake was minimal and
349 insufficient to raise the lake level above the groundwater level. Therefore, groundwater discharge into
350 the lake continued in May 2023. The simulated LGD rates ranged from 35.10 to 48.90 $mm \cdot d^{-1}$ between
351 August 2022 and May 2023 (Figure 3b), with an approximately 8% error compared to the rates derived
352 from the ^{222}Rn mass balance model. These rates exhibited an increasing trend followed by a decreasing
353 trend, peaking in the middle of the groundwater discharge period, and tapering at both the beginning
354 and end stages.

355 During the groundwater discharge period, the changes in precipitation and evaporation were
356 inversely related to the changes in LGD, demonstrating a clear negative correlation with LGD rates,
357 with correlation coefficients of R^2=0.61, $P < 0.01$ and R^2=0.67, $P < 0.01$, respectively (Figure 3b,
358 Figure S3 a and b). This suggested that lower monthly precipitation and evaporation contributed to the
359 larger LGD. This aligns with Jiang et al.'s (2024) results showing an inverse relationship between LGD

rates and precipitation/evaporation. Additionally, the value of precipitation minus evaporation (PME) played a significant role in the hydrological cycle. By analyzing the relationship between the PME and LGD rates, a non-linear relationship was identified, with the fitted equation being $Y=-0.0004X^2-0.0139X+47.08$, $R^2=0.86$, $P<0.05$ (Figure 3c). When PME was greater than 0, a larger PME resulted in a smaller LGD. When PME was less than 0, a smaller PME led to a smaller LGD. When both precipitation and evaporation were low and the PME approached 0, LGD reached its maximum value.

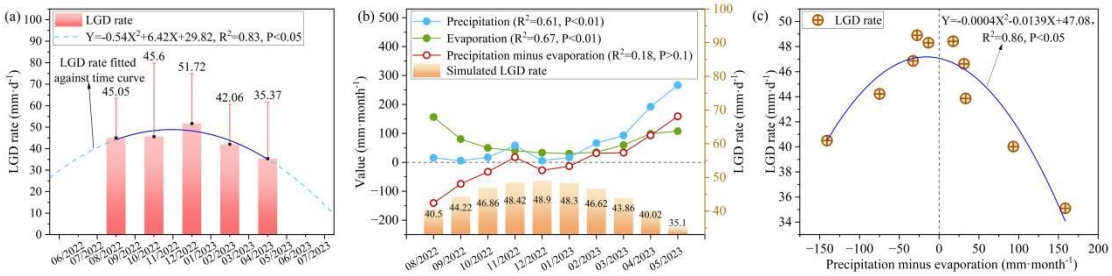

Figure 3. (a) The LGD rate of different periods and their fitted relationship between LGD rate and time. (b) Relationship between simulated LGD rate and precipitation and evaporation, where R^2 represents the linear correlation coefficient between this indicator and the LGD rate. (c) Relationship between PME and LGD rate.

3.2.2 Dominance of precipitation and evaporation on seasonal variations in LGD rates

At different periods, a strong correlation was observed between the LGD rate and hydraulic gradient ($R^2=0.77$, $P<0.05$) (Figure 4a), with both showing a consistent trend of change, in accordance with Darcy's law (Tecklenburg and Blume; 2017) (Figure 4a). The hydraulic gradient is controlled by the water level difference between groundwater and lake water—when this difference increases, the LGD rate rises; when it decreases, the LGD rate declines. From August to December 2022, the water level difference increased, leading to a rising LGD rate; from December 2022 to April 2023, the difference decreased, resulting in a lower LGD rate (Figure 4a). This variation is determined by the differences in groundwater level and lake water level. If the lake level drops more than the groundwater level, the gradient increases and LGD intensifies; if the groundwater level drops more, the gradient and LGD both decline (Figure 4b).

Monitoring data show that lake levels consistently declined during the study period, though the rate of decline slowed, primarily due to low precipitation, reduced evaporation, cooler temperatures, and decreased water consumption by agriculture and aquatic organisms. After February 2023, increasing precipitation slightly raised lake levels. Groundwater levels also declined steadily, mainly due to continuous LGD to lake, with minimal influence from human extraction or evaporation.

Between August and December 2022, groundwater levels fell more slowly than lake levels, increasing the hydraulic gradient and LGD. From February 2023 onward, the groundwater level declined more than the lake level, reducing the gradient and LGD rate. By April 2023, groundwater levels stabilized while lake levels rose slightly, further decreasing the hydraulic gradient and LGD.

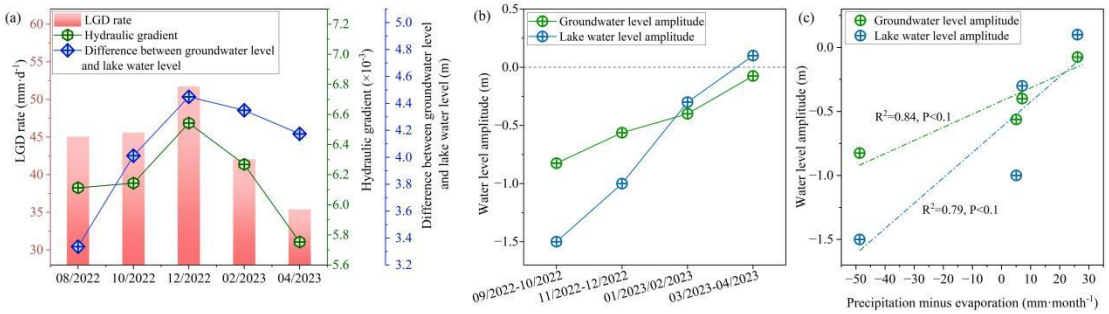

Figure 4. (a) Temporal characteristics of LGD rate, hydraulic gradient, and difference in groundwater and lake water levels. (b) Temporal characteristics of groundwater and lake water level change amplitudes, negative values indicate the amplitudes of water level decline, while positive values represent the amplitudes of water level rise. (c) Relationship between groundwater level amplitude, lake water level amplitude, and PME.

Net precipitation (PME) directly affects lake level fluctuations and indirectly influences groundwater levels by altering the water level difference (Figure 4c). A higher PME slows or reverses lake level decline, reducing groundwater discharge and limiting groundwater level drop. A lower PME accelerates lake level decline, enhancing groundwater discharge and deepening the groundwater level drop. Therefore, PME modulated the lake level changes, which subsequently influenced the groundwater levels, altered the lake-groundwater level difference, and regulated the hydraulic gradient, ultimately controlling the seasonal variations in LGD rates. A conceptual model of this mechanism is shown in Figure 5.

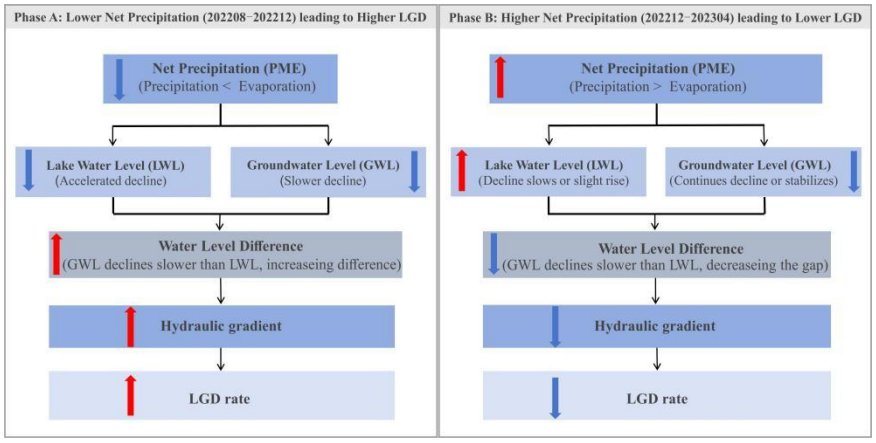

Figure 5. Conceptual model illustrating the mechanisms by which precipitation and evaporation influence LGD rates. Red upward arrows and blue downward arrows indicate increasing and decreasing trends of the corresponding parameters, respectively.

3.3 Impact of LGD-carried N and P on seasonal nutrient status of lakes

3.3.1 Seasonal variations in TN and TP loads carried by LGD

Between August 2022 and April 2023, the concentration of TN in the groundwater exhibited notable temporal variability, ranging from 0.24 to 0.46 $mmol \cdot L^{-1}$. The lowest concentration was observed in August 2022, whereas the peak was observed in December 2022 (Table 3). In comparison, the range of temporal variations in TP concentration in groundwater was wider, spanning from 6.46×10^{-3} to 2.19×10^{-2} $mmol \cdot L^{-1}$ (Table 3). The lowest TP concentration was recorded in December 2022, whereas the highest occurred in February 2023. Based on Eh, DO, and EC results (Table S3), TP concentration fluctuations likely result from the combined effects of internal adsorption and fixation, external input pulses, and geochemical competition under the background of an oxidation-enhanced environment driven by declining water levels (Eh and DO continuously increasing). For a detailed analysis, see the SI.

Table 3. Concentrations of TN and TP in groundwater at various periods and loads of TN and TP carried by LGD.

	TN concentration in groundwater ($mmol \cdot L^{-1}$)	TP concentration in groundwater ($mmol \cdot L^{-1}$)	LGD-TN ($mmol \cdot m^{-2} \cdot d^{-1}$)	LGD-TP ($mmol \cdot m^{-2} \cdot d^{-1}$)
08/2022	0.24	1.69×10^{-2}	10.76	0.76
10/2022	0.33	2.00×10^{-2}	15.22	0.91
12/2022	0.46	6.46×10^{-3}	24.00	0.33
02/2023	0.34	2.19×10^{-2}	14.25	0.92
04/2023	0.39	8.24×10^{-3}	13.93	0.29

Multiplying the LGD rate by the concentrations of TN and TP in the groundwater demonstrated the nutrient load carried by LGD. The variations in nutrient loads from August 2022 to April 2023 are shown in Figures 6d and 6e. The loads of TN carried by LGD (LGD-TN) ranged from 10.76 to 24.00 $mmol \cdot m^{-2} \cdot d^{-1}$, with the lowest load occurring in August 2022 and the highest in December 2022. Similarly, the loads of TP carried by LGD (LGD-TP) ranged from 0.29 to 0.92 $mmol \cdot m^{-2} \cdot d^{-1}$, with the highest load observed in December 2022 and the lowest in April 2023. The temporal variation in LGD-TN loads followed the trend of the LGD rate and was primarily influenced by the LGD rate. In contrast, the variation in LGD-TP loads over time did not align with the LGD rate and was mainly controlled by the concentration of TP in the groundwater.

3.3.2 Seasonal relationship between LGD-carried TN/TP loads and nutrient status of lakes

The nutrient status of lakes is determined by various parameters, and the concentration of Chl *a* in lake water is considered particularly important. In this study, no significant correlation was observed

between Chl *a* concentration and the concentrations of TN and TP (Figures 6a and 6b). However, a correlation was identified with the TN to TP molar ratio (TN/TP) (Figure 6c). As the TN/TP ratio approached the Redfield ratio of 16 (Figure 6c), the Chl *a* concentration increased (AC, 1960), whereas a deviation from this ratio was associated with a decrease in Chl *a* concentration, which was consistent with the findings reported in other studies (Qin et al., 2020).

In the absence of surface water inflow and pollutant discharge from prohibited human activities, N and P enter the lake primarily through groundwater discharge, atmospheric deposition, and sediment release. To quantify TN and TP inputs from atmospheric deposition and sediment release, comprehensive field monitoring and experimental investigations were conducted during HW lake periods (Tables S1 and S2). The results indicated that the TN and TP loads from atmospheric deposition were 0.09 and 9.68×10^{-4} $mmol\cdot m^{-2}\cdot d^{-1}$, respectively. Simultaneously, the diffusive TN and TP loads from lakebed sediment were 0.08 and 1.29×10^{-4} $mmol\cdot m^{-2}\cdot d^{-1}$, respectively. In contrast, the LGD-TN and LGD-TP loads were 1–2 orders of magnitude higher than those from atmospheric deposition and sediment release, indicating that LGD-TN and LGD-TP constituted the primary sources of TN and TP in the lake. A strong correlation was observed between LGD-TN loads and TN concentrations in lake water (R^2=0.79, P<0.05) (Figure 6d), whereas the LGD-TP loads exhibited entirely consistent variations with TP concentrations in lake water (R^2=0.89, P<0.05) (Figure 6e), highlighting their significant influence.

The molar ratio of TN to TP in LGD (LGD-TN/TP) exhibited variations that were entirely consistent with the TN/TP ratio in the lake water, indicating a strong correlation (R^2=0.82, P<0.05) (Figure 6f), thereby indicating its regulatory effect on the lake water TN/TP ratio. Based on the observed changes in LGD-TN/TP and their reflection in lake water TN/TP, when the lake water TN/TP reached 15.35 in April 2023, the Chl *a* concentration was elevated. These results demonstrated that the LGD-derived TN and TP substantially influenced the lake's nutrient status by modulating the TN/TP ratio, thereby affecting the Chl *a* concentration and the overall nutrient balance.

In addition, light availability and water temperature can also affect Chl *a* growth. Although higher temperatures and favorable light conditions in summer and autumn are theoretically conducive to phytoplankton proliferation, Figure. 6f shows that Chl *a* concentrations decreased continuously from August 2022 to February 2023, but increased rapidly and reached a peak in April 2023. This increase may be partly related to improvements in light and temperature conditions. However, during the

summer wet season, when temperature and light are most favorable and LGD is absent, the mean Chl *a* concentration was only ~60 μg/L, which is much lower than the 98.69 μg/L observed in April 2023. These results suggest that light and temperature are not the dominant drivers of Chl *a* variability; instead, nitrogen and phosphorus concentrations and their TN/TP are the key controlling factors.

In lake eutrophication management, Chl *a* accumulation is governed not only by the absolute concentrations of nitrogen and phosphorus but also by the TN/TP, which determines the dominant type of nutrient limitation. Low TN/TP indicate nitrogen limitation, whereas high TN/TP indicate phosphorus limitation. Given that present study has shown that groundwater can significantly alter lake TN/TP, its influence should be explicitly considered when identifying nutrient limitation mechanisms and developing targeted nitrogen and phosphorus reduction strategies.

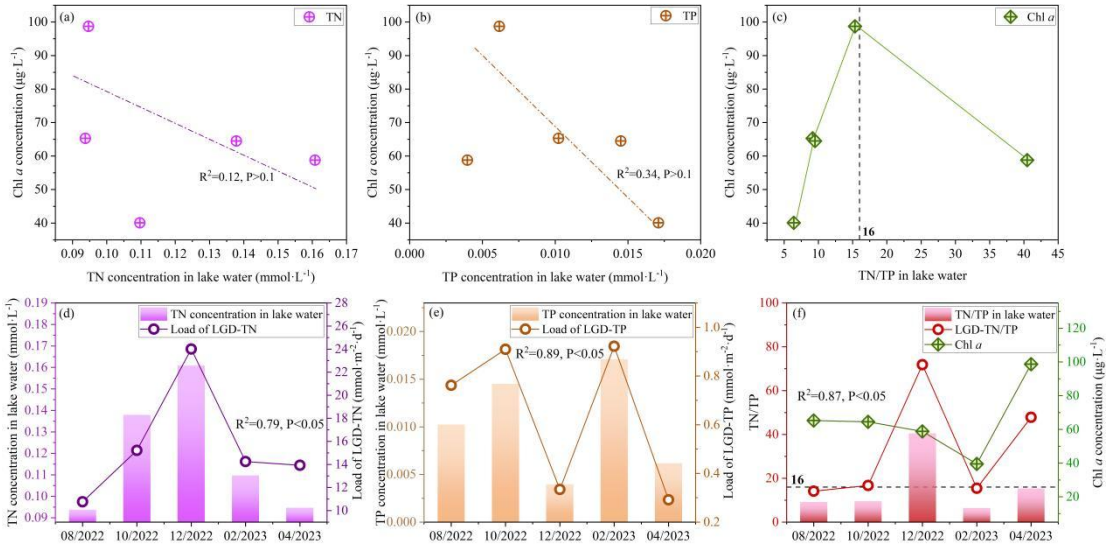

Figure 6. Relationship between LGD-TN and TP loads and lake water TN and TP concentrations, as well as the lake water Chl *a* concentration. (a) Relationship between Chl *a* concentration and lake water TN concentration. (b) Relationship between Chl *a* concentration and lake water TP concentration. (c) Relationship between Chl *a* concentration and lake water TN/TP. (d) Relationship between lake water TN concentration and LGD-TN load. (e) Relationship between lake water TP concentration and LGD-TP load. (f) Relationship between lake water TN/TP and LGD-TN/TP load.

3.4 Implications

3.4.1 Advantages of high-frequency observations in LGD research

Traditional low-frequency sampling (e.g., single or quarterly measurements) has difficulty capturing short-term variations in LGD and its coupling with short-term meteorological conditions and water-level fluctuations. High-frequency observations can capture LGD responses to environmental factors such as meteorology and water temperature over relatively short timescales, and provide higher-resolution hydrological time series, thereby supplying reliable data for accurate estimation of LGD rates. In addition, high-frequency observations can record the short-term contributions of LGD to

lake N and P inputs, enabling more precise flux assessments, avoiding biases associated with low-frequency sampling, and revealing the response relationships between LGD and Chl *a* concentrations or algal bloom events. Based on high-frequency data, LGD predictive models that account for the coupling of meteorological and hydrological factors can also be developed. Therefore, in LGD research, high-frequency observations are of significant value for accurately quantifying the impacts of groundwater on lake aquatic ecosystems and should be given priority.

3.4.2 Dominant factors controlling the seasonal variability of LGD

The seasonal variability of LGD is primarily governed by three categories of factors—meteorological, hydrological, and anthropogenic—with the dominant controls differing across lake types.

(1) In open lakes (e.g., Poyang Lake and Tonle Sap Lake), hydrological processes dominate LGD dynamics. Their hydraulic connection with external rivers (such as the Yangtze and Mekong Rivers) causes rapid lake-level rises during the wet season and pronounced declines during the dry season, thereby modifying the hydraulic gradients between the littoral zone and aquifer and directly regulating groundwater discharge rates (Burnett et al. 2017; Li et al. 2020). (2) In closed lakes, where external fluvial influence is minimal, LGD dynamics are primarily controlled by the balance between precipitation and evaporation. Previous studies (Shi et al., 2022; Gan et al., 2024) have shown that under relatively stable groundwater levels, strong evaporation lowers lake levels, steepens the hydraulic gradient, and enhances LGD, whereas precipitation-dominated periods raise lake levels and suppress LGD. Hence, the seasonal oscillation of LGD in closed-basin systems essentially reflects a periodic adjustment of lake–groundwater hydraulic connectivity driven by meteorological forcing. (3) Anthropogenic activities, such as artificial water regulation and groundwater abstraction, can further modify LGD by altering regional hydrological circulation and the hydraulic relationships between lakes and aquifers (Xiong et al., 2023).

3.4.3 Regulatory role of LGD in lake nutrient status

In closed lakes lacking significant surface inflow, LGD not only constitutes a key component of the water balance but also plays a pivotal role in nutrient transport and water quality evolution. The nitrogen and phosphorus fluxes carried by LGD directly influence the spatial and temporal patterns of

nutrient concentrations and Chl *a* within the lake. Several studies support this mechanism. For instance, Xu et al. (2024) showed that in small semi-arid lakes, LGD inputs largely determine the spatial distribution of Chl *a*, while Shi et al. (2022) reported a delayed response of lake trophic conditions to LGD-derived nutrient inputs. Such lakes are typically characterized by strong enclosure and long water residence times, conditions that amplify the influence of groundwater in biogeochemical cycling and ecological processes.

Synthesizing current knowledge, the linkage from seasonal forcing to ecological response in closed lakes can be conceptualized as follows: meteorological conditions (precipitation–evaporation balance) serve as the initial driver, regulating lake–groundwater hydraulic gradients and thereby controlling the seasonal magnitude of LGD. LGD, in turn, acts as a key conduit for nutrient fluxes, with its temporal variability shaping nutrient and Chl *a* distributions and ultimately modulating nutrient dynamics.

Previous studies have long approached the issue of internal nutrient loading in lakes primarily from the perspective of nitrogen and phosphorus release from bottom sediments, emphasizing the role of sediment-derived nutrients in shaping lake trophic status (Donohue and Garcia Molinos, 2009). For lakes where LGD-derived nutrient loads are relatively small during specific seasons, sedimentary nutrient release can indeed constitute a major source to the overlying water column, consistent with traditional understanding (Xu et al., 2017). However, in systems where LGD inputs are substantial, focusing solely on sedimentary release may not fully capture the true structure of lake nutrient sources. Although systematic studies that simultaneously assess both sediment nutrient release and LGD-derived inputs remain limited, existing evidence indicates that LGD is likely a key mechanism sustaining nutrient cycling and ecological succession in closed-basin lakes, highlighting the need for more comprehensive and quantitative investigations.

HW lake and other study cases are all typical closed shallow lakes, with limited exchange between the lake water and surface inflows, making LGD the primary hydrological input. A large number of similar lakes exist worldwide (e.g., closed lakes in the North American Great Plains, inland lakes in Africa and Central Asia), which may also be significantly influenced by LGD. Moreover, the regulatory effect of LGD on the spatial distribution of nitrogen, phosphorus, Chl *a*, and algal growth is amplified in lakes with long water residence times and stable sediment–water exchange. Therefore, this mechanism can be extended to other closed shallow lakes, particularly those with pronounced seasonal

554 climates and a high proportion of shallow areas.

555

556 **3.4.4 Future recommendations for the lake management of closed shallow lakes**

557 Based on the above understanding, future research should adopt a systems-based perspective,
558 focusing on comparative analyses of LGD inputs versus internal sediment release and quantitatively
559 identifying their relative importance across different lake types and temporal scales to clarify the
560 primary nutrient sources. This approach can provide a scientific basis for designing targeted nitrogen
561 and phosphorus reduction strategies, as well as effective lake management and ecological restoration
562 measures, thereby improving water quality and ecological function in closed lakes.

563 Moreover, climate change is expected to modulate these processes. In the East Asian monsoon
564 region, future precipitation is projected to become more concentrated in summer, while non-summer
565 periods, particularly autumn and winter, may experience reduced rainfall and increased evaporation.
566 Because LGD predominantly occurs during non-summer periods, increased net precipitation
567 (precipitation minus evaporation) could enhance groundwater discharge, directly elevating associated
568 TN and TP fluxes. These considerations further underscore the critical role of groundwater in
569 regulating nutrient balances in closed lakes and highlight the need for future nutrient management
570 strategies to account for both LGD variability and climate-driven hydrological changes.

571

572 **4 Conclusions**

573 High-frequency monitoring and hydrochemical methods were employed to investigate the
574 dynamics of LGD and associated nutrient loads in Heiwawu Oxbow Lake from August 2022 to April
575 2023, revealing the regulatory mechanisms of precipitation-evaporation processes. The LGD flux
576 exhibited an increasing-then-decreasing trend during the study period, ranging from 35.36 to 51.71
577 $mm \cdot d^{-1}$, with a peak in December 2022 and a minimum in April 2023. The LGD rates were governed
578 by the hydraulic gradient between groundwater and lake water, which responded nonlinearly to net
579 monthly precipitation. Positive net precipitation induced rapid lake recharge, reduced the hydraulic
580 gradient, and suppressed LGD rates. Conversely, negative net precipitation enhanced
581 evaporation-driven lake discharge, steepened the hydraulic gradient, and increased LGD rates. When
582 net precipitation approached zero, a critical hydraulic equilibrium was reached, yielding the highest
583 LGD rates. The LGD was also a major nutrient pathway, with TN and TP loads significantly correlating

with lake concentrations. The TN/TP ratio of LGD aligned with lake water, influencing phytoplankton structure and Chl *a* levels. This study reveals the regulatory mechanisms by which LGD is controlled by the precipitation–evaporation balance at the monthly scale, quantitatively evaluates the impacts of groundwater-driven nutrient transport on lake eutrophication, and, by reference to related global case studies, provides environmental protection and management implications from a groundwater perspective. These findings offer new insights into eutrophication control in closed, shallow lakes, and suggest that the advantages of high-frequency LGD observations should be incorporated into lake management frameworks, along with the development of targeted control strategies during critical periods of groundwater–lake interactions.

Acknowledgments

The research was funded by National Natural Science Foundation of China (Nos. 42422707, U21A2026), and Fundamental and Interdisciplinary Disciplines Breakthrough Plan of the Ministry of Education of China (No. JYB2025XDXM911). The authors would like to thank all the reviewers who participated in the review, as well as MJEditor (www.mjeditor.com) for providing English editing services during the preparation of this manuscript.

Declaration of interests

The authors declare that they have no known competing financial interests or personal relationships.

Data Availability Statement

Data will be made available on request.

Author contributions

Writing-review & editing, Writing-original draft, Methodology, Investigation, Data curation: XS. Writing-review & editing, Resources, Methodology, Funding acquisition: YD. Investigation: HT, JX, HS, YL. Project administration: YD. Funding acquisition: YG. Resources, Project administration: YW.

References

Redfield, A. C.: The biological control of chemical factors in the environment, Sci. Prog., 11, 150–170,

1960.

Adyasari, D., Dimova, N. T., Dulai, H., Gilfedder, B. S., Cartwright, I., McKenzie, T., and Fuleky, P.: Radon-222 as a groundwater discharge tracer to surface waters, Earth-Sci. Rev., 238, 104321, https://doi.org/10.1016/j.earscirev.2023.104321, 2023.

Arnoux, M., Gibert-Brunet, E., Barbecot, F., Guillon, S., Gibson, J., and Noret, A.: Interactions between groundwater and seasonally ice-covered lakes: using water stable isotopes and radon-222 multilayer mass balance models, Hydrol. Process., 31, 2566–2581, https://doi.org/10.1002/hyp.11206, 2017.

Burnett, W. C., Wattayakorn, G., Supcharoen, R., Sioudom, K., Kum, V., Chanyotha, S., and Kritsananuwat, R.: Groundwater discharge and phosphorus dynamics in a flood-pulse system: Tonle Sap Lake, Cambodia, J. Hydrol., 549, 79–91, https://doi.org/10.1016/j.jhydrol.2017.03.049, 2017.

Corbett, D.R, Burnett, W., Cable, P., Clark, S.: A multiple approach to the determination of radon fluxes from sediments. Journal of Radioanalytical and Nuclear Chemistry, 236(1–2), 247–253, https://doi.org/10.1007/bf02386351, 1998.

Dabrowski, J. S., Charette, M. A., Mann, P. J., Ludwig, S. M., Natali, S. M., Holmes, R. M., and Henderson, P. B.: Using radon to quantify groundwater discharge and methane fluxes to a shallow, tundra lake on the Yukon–Kuskokwim Delta, Alaska, Biogeochemistry, 148, 69–89, https://doi.org/10.1007/s10533-020-00647-w, 2020.

Dimova, N. T. and Burnett, W. C.: Evaluation of groundwater discharge into small lakes based on the temporal distribution of radon-222, Limnol. Oceanogr., 56, 486–494, https://doi.org/10.4319/lo.2011.56.2.0486, 2011.

Donohue, I., and Garcia Molinos, J.: Impacts of increased sediment loads on the ecology of lakes. Biological reviews, 84(4), 517-531, https://doi.org/10.1111/j.1469-185X.2009.00081.x, 2009.

Gan, Y., Sun, X., Wu, J., Du, Y., Deng, Y., Han, P., and Wang, Y.: Spatio-temporal variations of lacustrine groundwater discharge and related nutrient fluxes in a typical lake in front of hillocks, J. Hydrol., 635, 131166, https://doi.org/10.1016/j.jhydrol.2024.131166, 2024.

Gao, X., Jia, T., Xu, Q., Wang, F., and Wang, A.: Records of lacustrine sedimentology and pollen–charcoal assemblages responding to climate change and human activities in Zhongzhouzi Oxbow Lake, Hubei Province for about 70 years, Quaternary Sci., 36, 1445–1455,

https://doi.org/10.11928/j.issn.1001-7410.2016.06.10, 2016.

Gonneea, M. E., Morris, P. J., Dulaiova, H., and Charette, M. A.: New perspectives on radium behavior within a subterranean estuary, Mar. Chem., 109, 250–267, https://doi.org/10.1016/j.marchem.2007.12.002, 2008.

Hu, M., Zhou, P., and Chen, C.: Study on coupling of typical elements in surface water and groundwater in the middle reaches of the Yangtze River, China, J. Hydrol., 623, 130298, https://doi.org/10.1016/j.jhydrol.2023.130298, 2023.

Jia, T., Wang, F., and Yuan, S.: Sedimentation and its environmental significance of the Niuyu Lake along the middle reaches of the Yangtze River: a case study of Tian'e Island and Zhongzhouzi in the Jingjiang section of the Yangtze River, Geogr. Res., 34, 861–871, 2015. (in Chinese)

Jiang, C., Jiang, C., Wang, Q., Liu, H., Li, D., Zhu, Q., and Liu, F.: Seasonal characteristics of groundwater discharge controlled by precipitation and its environmental effects in a coal mining subsidence lake, eastern China, Sci. Total Environ., 915, 170067, https://doi.org/10.1016/j.scitotenv.2024.170067, 2024.

Jiang, X., Ma, R., Ma, T., and Sun, Z.: Modeling the effects of water diversion projects on surface water and groundwater interactions in the central Yangtze River Basin, Sci. Total Environ., 830, 154606, https://doi.org/10.1016/j.scitotenv.2022.154606, 2022.

Kazmierczak, J., Postma, D., Muller, S., Jessen, S., Nilsson, B., Czekaj, J., and Engesgaard, P.: Groundwater-controlled phosphorus release and transport from sandy aquifer into lake, Limnol. Oceanogr., 65, 1447–1463, https://doi.org/10.1002/lno.11447, 2020.

Kluge, T., Ilmberger, J., von Rohden, C., and Aeschbach-Hertig, W.: Tracing and quantifying groundwater inflow into lakes using a simple method for radon-222 analysis, Hydrol. Earth Syst. Sci., 11, 1621–1631, https://doi.org/10.5194/hess-11-1621-2007, 2007.

Lewandowski, J., Rosenberry, D. O., and Meinikmann, K.: Groundwater–lake interfaces, in: Ecohydrological Interfaces, edited by: Krause, S., Hannah, D. M., and Fleckenstein, J. H., Wiley, Hoboken, NJ, 103–122, https://doi.org/10.1002/9781119639308.ch6, 2024.

Luo, X., Kuang, X. X., Jiao, J. J., Liang, S. H., Mao, R., Zhang, X. L., and Li, H. L.: Evaluation of lacustrine groundwater discharge, hydrologic partitioning, and nutrient budgets in a proglacial lake in the Qinghai–Tibet Plateau using 222Rn and stable isotopes, Hydrol. Earth Syst. Sci., 22, 5579–5598, https://doi.org/10.5194/hess-22-5579-2018, 2018.

675 MacIntyre, S., Wanninkof, R., & Chanton, J.P.: Trace gas exchange across the air-water interface in
676 freshwater and coastal marine environments, in, edited by: Matson, PA and Harriss, RC, Biogenic
677 trace gases: Measuring emissions from soil and water, Methods Ecol. Evol, 52–97, 1995.
678 Meinikmann, K., Hupfer, M., and Lewandowski, J.: Phosphorus in groundwater discharge – a potential
679 source for lake eutrophication, J. Hydrol., 524, 214–226,
680 https://doi.org/10.1016/j.jhydrol.2015.02.031, 2015.
681 Olid, C., Rodellas, V., Rocher-Ros, G., Garcia-Orellana, J., Diego-Feliu, M., Alorda-Kleinglass, A.,
682 Bastviken, D., and Karlsson, J.: Groundwater discharge as a driver of methane emissions from
683 Arctic lakes, Nat. Commun., 13, 3667, https://doi.org/10.1038/s41467-022-31219-1, 2022.
684 Petermann, E., Gibson, J. J., Knöller, K., Pannier, T., Weiß, H., and Schubert, M.: Determination of
685 groundwater discharge rates and water residence time of groundwater-fed lakes by stable isotopes
686 of water (18O, 2H) and radon (222Rn) mass balances, Hydrol. Process., 32, 805–816,
687 https://doi.org/10.1002/hyp.11401, 2018.
688 Qin, B., Zhou, J., Elser, J. J., Gardner, W. S., Deng, J., and Brookes, J. D.: Water depth underpins the
689 relative roles and fates of nitrogen and phosphorus in lakes, Environ. Sci. Technol., 54, 3191–3198,
690 https://doi.org/10.1021/acs.est.9b05835, 2020.
691 Rosenberry, D. O., Lewandowski, J., Meinikmann, K., and Nützmann, G.: Groundwater – the
692 disregarded component in lake water and nutrient budgets. Part 1: effects of groundwater on
693 hydrology, Hydrol. Process., 29, 2895–2921, https://doi.org/10.1002/hyp.10403, 2015.
694 Schmidt, A., Gibson, J. J., Santos, I. R., Schubert, M., Tattrie, K., and Weiss, H.: The contribution of
695 groundwater discharge to the overall water budget of two typical boreal lakes in Alberta, Canada
696 estimated from a radon mass balance, Hydrol. Earth Syst. Sci., 14, 79–89,
697 https://doi.org/10.5194/hess-14-79-2010, 2010.
698 Shi, X., Luo, X., Jiao, J. J., and Zuo, J.: Dominance of evaporation on lacustrine groundwater discharge
699 to regulate lake nutrient state and algal blooms, Water Res., 219, 118620,
700 https://doi.org/10.1016/j.watres.2022.118620, 2022.
701 Stets, E. G., Winter, T. C., Rosenberry, D. O., and Striegl, R. G.: Quantification of surface water and
702 groundwater flows to open- and closed-basin lakes in a headwaters watershed using a descriptive
703 oxygen stable isotope model, Water Resour. Res., 46, W03504,
704 https://doi.org/10.1029/2009WR007793, 2010.

Sun, X., Du, Y., Deng, Y., Fan, H., Tao, Y., and Ma, T.: Contribution of groundwater discharge and associated contaminants input to Dongting Lake, Central China, using multiple tracers (222Rn, 18O, Cl−), Environ. Geochem. Health, 43, 1239–1255, https://doi.org/10.1007/s10653-020-00647-3, 2021.

Sun, X., Du, Y., Wu, J., Xu, J., Tian, H., Deng, Y., and Wang, Y.: Two-decadal variability of lacustrine groundwater discharge: coupled controls from weather and hydrologic changes, Water Resour. Res., 60, e2024WR037173, https://doi.org/10.1029/2024WR037173, 2024.

Sun, X., Du, Y., Wu, J., Xu, J., Tian, H., Han, P., and Wang, Y.: Spatial variability of lacustrine groundwater discharge at basin scale, J. Hydrol., 629, 134404, https://doi.org/10.1016/j.jhydrol.2024.134404, 2025a.

Sun, X., Du, Y., Xu, J., Tian, H., Deng, Y., Gan, Y., and Wang, Y.: Control of groundwater–lake interaction zone structure on spatial variability of lacustrine groundwater discharge in oxbow lake, Water Resour. Res., 61, e2024WR039334, https://doi.org/10.1029/2024WR039334, 2025b.

Tecklenburg, C. and Blume, T.: Identifying, characterizing and predicting spatial patterns of lacustrine groundwater discharge, Hydrol. Earth Syst. Sci., 21, 5043–5063, https://doi.org/10.5194/hess-21-5043-2017, 2017.

Walvoord, M. A. and Striegl, R. G.: Increased groundwater to stream discharge from permafrost thawing in the Yukon River basin: potential impacts on lateral export of carbon and nitrogen, Geophys. Res. Lett., 34, L12402, https://doi.org/10.1029/2007GL030216, 2007.

Wang, Q., Li, H., Zhang, Y., Wang, X., Zhang, C., Xiao, K., and Qu, W.: Evaluations of submarine groundwater discharge and associated heavy metal fluxes in Bohai Bay, China, Sci. Total Environ., 695, 133873, https://doi.org/10.1016/j.scitotenv.2019.133873, 2019.

Webster, I. T., Hancock, G. J., and Murray, A. S.: Modelling the effect of salinity on radium desorption from sediments, Geochim. Cosmochim. Acta, 59, 2469–2476, https://doi.org/10.1016/0016-7037(95)00111-7, 1995.

Xiong, L., Aldahan, A., Qian, R., Yi, P., Chen, X., Li, K., and He, P.: Spatio-temporal patterns and quantification of lake–groundwater interaction determined in a large water transfer lake, Hydrol. Process., 37, e14867, https://doi.org/10.1002/hyp.14867, 2023.

Xu, R., Du, Y., Wang, Z., Sun, X., Yang, L., Liu, J., and Gan, Y.: Contrasting lacustrine groundwater discharge in two small perennial lakes around dried-up Chahannaoer Lake, Northern China, J.

735 Hydrol. Reg. Stud., 58, 102280, https://doi.org/10.1016/j.ejrh.2025.102280, 2025.
736 Xu, Y., Wu, Y., Han, J., and Li, P.: The current status of heavy metal in lake sediments from China:
737 Pollution and ecological risk assessment. Ecology and evolution, 7(14), 5454-5466.
738 https://doi.org/10.1002/ece3.3124, 2017.
739 Xue, P., Wen, Z., Zhao, D., Jakada, H., and Liang, X.: Determination of hydraulic conductivity and its
740 spatial variability in the Jianghan Plain using a multi-format, multi-method approach, J. Hydrol.,
741 594, 125917, https://doi.org/10.1016/j.jhydrol.2021.125917, 2021.
742 Zedler, J. B. and Kercher, S.: Wetland resources: status, trends, ecosystem services, and restorability,
743 Annu. Rev. Environ. Resour., 30, 39–74,
744 https://doi.org/10.1146/annurev.energy.30.050504.144248, 2005.
745 Zheng, J., Chen, K., Wu, J., and Wu, J.: Lacustrine groundwater discharge as an important hidden
746 source of nutrients to a large eutrophic lake: implications for eutrophication management, Sci.
747 Total Environ., 960, 178313, https://doi.org/10.1016/j.scitotenv.2024.178313, 2025.